ADVANCED INTELLIGENT SYSTEMS
Open Access
www.advintellsyst.com

Experimental Estimation of Gap Thickness and Electrostatic Forces Between Contacting Surfaces Under Electroadhesion

*Easa AliAbbasi, Ørjan Grottem Martinsen, Fred-Johan Pettersen, James Edward Colgate, and Cagatay Basdogan**

Electroadhesion (EA) is a promising technology with potential applications in robotics, automation, space missions, textiles, tactile displays, and some other fields where efficient and versatile adhesion is required. However, a comprehensive understanding of the physics behind it is lacking due to the limited development of theoretical models and insufficient experimental data to validate them. This article proposes a new and systematic approach based on electrical impedance measurements to infer the electrostatic forces between two dielectric materials under EA. The proposed approach is applied to tactile displays, where skin and voltage-induced touchscreen impedances are measured and subtracted from the total impedance to obtain the remaining impedance to estimate the electrostatic forces between the finger and the touchscreen. This approach also marks the first instance of experimental estimation of the average air gap thickness between a human finger and a voltage-induced capacitive touchscreen. Moreover, the effect of electrode polarization impedance on EA is investigated. Precise measurements of electrical impedances confirm that electrode polarization impedance exists in parallel with the impedance of the air gap, particularly at low frequencies, giving rise to the commonly observed charge leakage phenomenon in EA.

1. Introduction

Electroadhesion (EA) refers to the attraction between two dielectric materials due to an applied electric field.[1–3] As shown in **Figure 1**a, the high voltage applied to the electrodes embedded in dielectric 1 results in accumulation of electrical charges in it. Once dielectric 1 contacts dielectric 2, induced charges with opposite polarities accumulate at the interface of dielectric 2. The opposite charges at the interfaces of the dielectrics attract each other and result in electrostatic forces due to the nonuniform air gap between them.

The discovery of EA can be traced back to 1923 when Frederik Alfred Johnsen and Knud Rahbek,[4] two Danish engineers, observed an adhesive force between a brass plate and a slab of limestone resting on a voltage-induced conductor surface. Later, Mallinckrodt et al.[5] accidentally discovered in the 1950s that there was a sense of adhesion when a human finger explored a smooth metal surface coated with an insulating layer and connected to an AC source. This phenomenon was attributed to the principle of parallel-plate capacitors, wherein the metal surface and the human finger were treated as two parallel plates of a capacitor attracting each other. Since then, broad ranges of applications of EA have been introduced in various fields[3,6–13] (see Figure 1b). EA became commercially viable for industrial applications in the 1960s with the introduction of electrostatic plotters.[14] Around the same time, NASA started to employ EA technology in space missions for material handling[15] and later controllable earth orbit grappling and soft docking.[16,17] After a decade, EA entered the semiconductor industry with applications in material handling by using the devices commercially known as electrostatic chucks.[18–20] Starting from the 1990s, EA was first

E. AliAbbasi, C. Basdogan
College of Engineering
Koc University
Istanbul 34450, Turkey
E-mail: cbasdogan@ku.edu.tr

The ORCID identification number(s) for the author(s) of this article can be found under https://doi.org/10.1002/aisy.202300618.

© 2024 The Authors. Advanced Intelligent Systems published by Wiley-VCH GmbH. This is an open access article under the terms of the Creative Commons Attribution License, which permits use, distribution and reproduction in any medium, provided the original work is properly cited.

DOI: 10.1002/aisy.202300618

Ø. G. Martinsen, F.-J. Pettersen
Department of Physics
University of Oslo
Sem Sælands vei 24, 0371 Oslo, Norway

Ø. G. Martinsen, F.-J. Pettersen
Department of Clinical and Biomedical Engineering
Oslo University Hospital
0424 Oslo, Norway

J. E. Colgate
Department of Mechanical Engineering
Northwestern University
Evanston, IL 60208, USA

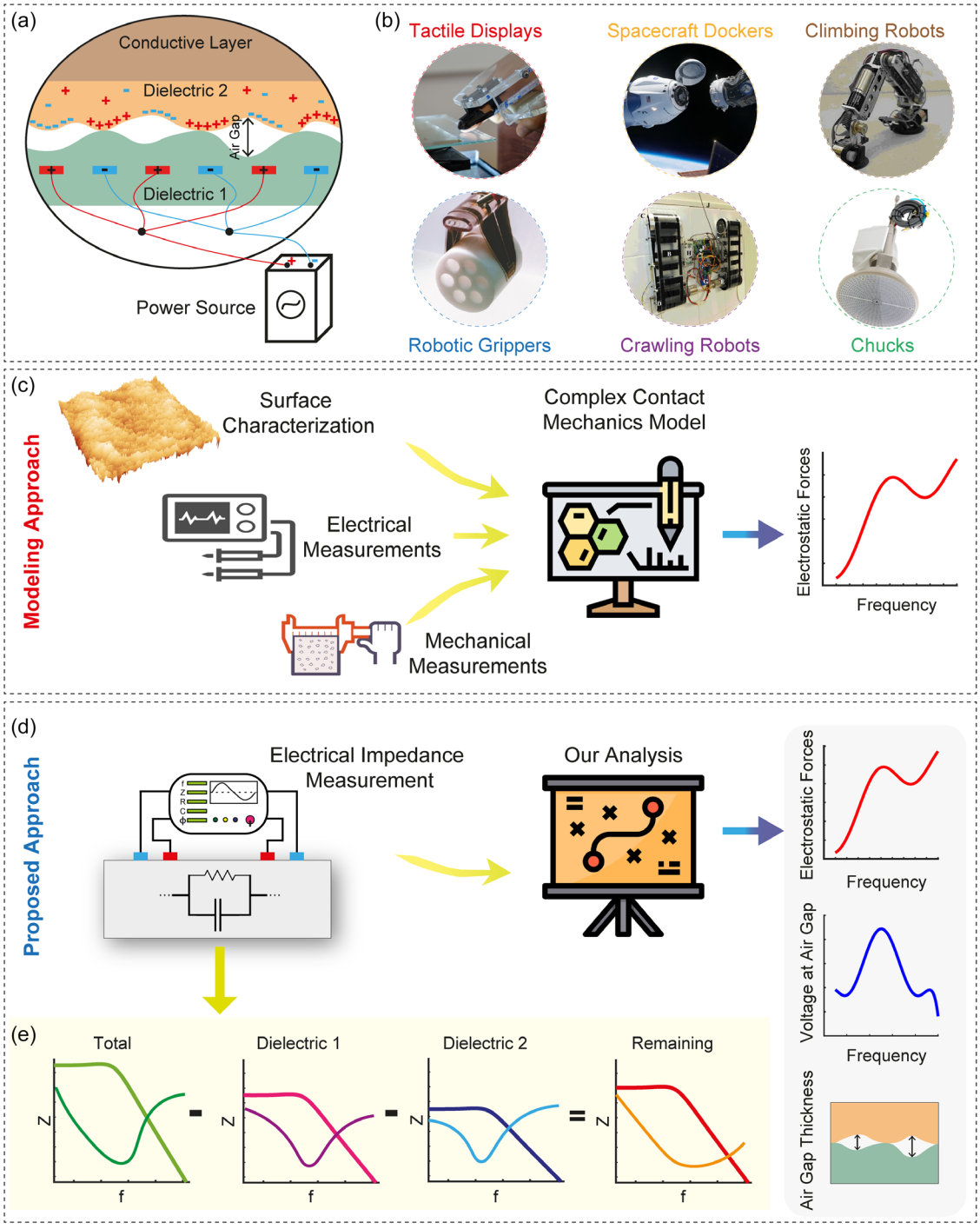


Figure 1. a) Schematic representation of electroadhesive devices. Dielectric 1 is in contact with dielectric 2, and there is an air gap between them due to their surface roughness. The electrodes embedded in dielectric 1 are connected to the power source, and hence induced electrical charges are accumulated at the interface of dielectric 2. The opposite charges at the interfaces of the dielectrics generate electrostatic forces and attract the dielectrics to each other. b) The EA technology has applications in tactile displays, spacecraft docking, climbing and crawling robots, robotic grippers, electrostatic chucks, etc. Reproduced with permission.[6] Copyright 2023, Wiley,[61] Copyright 2023, Wiley, and[62] Copyright 2023, Elsevier. c) Modeling approaches for calculating electrostatic forces require surface characterization and electrical and mechanical measurements. d) Our proposed approach for inferring the electrostatic forces, along with the air gap thickness, is based on electrical impedance measurements. e) In our approach, the impedances of dielectrics 1 and 2 are subtracted from the total impedance of the coupled system to obtain the remaining impedance, which enables us to infer the air gap thickness first and then the magnitude of electrostatic forces.

© 2024 The Authors. Advanced Intelligent Systems published by Wiley-VCH GmbH

26404567, 2024, 4, Downloaded from https://onlinelibrary.wiley.com/doi/10.1002/aisy.202300618 by Koc University, Wiley Online Library on [05/07/2024]. See the Terms and Conditions (https://onlinelibrary.wiley.com/terms-and-conditions) on Wiley Online Library for rules of use; OA articles are governed by the applicable Creative Commons License

26404567, 2024, 4, Downloaded from https://onlinelibrary.wiley.com/doi/10.1002/aisy.202300618 by Koc University, Wiley Online Library on [05/07/2024]. See the Terms and Conditions (https://onlinelibrary.wiley.com/terms-and-conditions) on Wiley Online Library for rules of use; OA articles are governed by the applicable Creative Commons License

embedded into the end effectors of robots for gripping composites and fibrous materials like fabric[21] and carbon fibers[22,23] and then later crawling and wall climbing robots[24–27] and into soft robotics[6,28–30] More recently, it was utilized in touch surfaces of mobile devices for displaying haptic feedback to the user with potential applications in many new domains (see the review of surface haptics in ref. [9]). The readers may refer to ref. [3,31] for a more comprehensive review of EA applications in robotics, including the ones in haptics.

The research on EA has experienced a growth rate of approximately 10% in annual publications over the past 60 years.[3] It has successfully entered various fields due to its unique benefits, which are difficult or even impossible to achieve through some other techniques, such as magnetic adhesion. For instance, electroadhesive devices can adhere to both conductive and insulating surfaces. They are compatible with vacuum environments since the gap between the contacting surfaces under EA is typically filled with air and its permittivity is almost equal to that of the vacuum. Additionally, EA consumes ultralow energy in some applications compared to its alternatives due to driving a small amount of current (see for example robotic insect application in ref. [32]). Some of the electroadhesive devices are also lightweight and less complex compared to some mechanical devices utilizing vacuum pumps and motors for the same purpose (e.g., material handling applications).

Despite the advantages of EA, there is a lack of comprehensive understanding of the physics behind it, which involves electrical and mechanical interactions between the contacting surfaces.[33] Moreover, our knowledge of the parameters influencing the magnitude of electrostatic forces that attract these surfaces to each other is highly limited. Designing controlled experiments to investigate the effects of these parameters on EA is not trivial due to the complex nature of the contact problem. Hence, there is insufficient experimental data on this topic in the literature. Furthermore, it is difficult to develop mathematical models to estimate electrostatic forces since the thickness of the air gap between the contacting surfaces is not uniform and changes with the input voltage and frequency, mechanical, and electrical properties of the contacting objects and their surface topography, initial contact forces, environmental factor, etc. (see Figure 1c). In addition, the polarization and depolarization of dielectrics in response to changes in the electric field as a function of frequency further complicates the modeling problem. Finally, the charge leakage through the contacting surfaces due to the differences in their electrical properties is not trivial to measure or model, despite its noticeable effects on the electrostatic forces.[34] To the best of our knowledge, there is no study in the literature clearly explaining the reasons behind this leakage phenomenon.

The electrostatic forces between the contacting surfaces can be calculated using the normal component of Maxwell's stress tensor[35]

$$F_{\mathrm{e}} = \frac{1}{2}\varepsilon_0 A_{\mathrm{app}} \frac{1}{u^2} \Delta V_{\mathrm{gap}}^2 \tag{1}$$

where ε_0, A_{app}, ΔV_{gap}, and u are the permittivity of free space ($8.854 \times 10^{-12}\,\mathrm{F\,m^{-1}}$), apparent contact area, the voltage at the air gap, and average air gap thickness, respectively. Equation (1) indicates that the magnitude of electrostatic force is proportional to the square of the voltage at the air gap and inversely proportional to the square of its thickness. It is worth mentioning here that the voltage term in Maxwell's stress tensor is the voltage at the air gap and not equal to the voltage applied to the electrodes, as the voltage drops at the dielectric layers must be accounted for. Furthermore, even if the contacting surfaces appear smooth, they have finite roughness at different length scales, resulting in a nonuniform air gap between the dielectrics.[36] Since this gap typically varies from a few nanometers to a few micrometers across the dielectrics, there is currently no direct experimental approach to measure the voltage at the air gap and the thickness of this gap to infer the electrostatic forces using Equation (1).

In this study, we present a systematic experimental approach to infer 1) the average thickness of the air gap; 2) the magnitude of the voltage at the air gap; and 3) the magnitude of the electrostatic forces between the contacting dielectrics based on the measurement of electrical impedances. The overview of the proposed approach is presented in Figure 1d. Typically, the total impedance of the interface shown in Figure 1a equals the summation of the impedances of dielectrics 1 and 2 and what we call the remaining impedance (see Figure 1e). The remaining term in this study represents the impedances of the air gap and the electrode polarization. Shultz et al.[37] considered the air gap impedance as the only remaining impedance and ignored the electrode polarization impedance. This electrode polarization impedance, due to what is known as "electric double layer" (EDL),[38] explains the charge leakage phenomenon reported in our earlier study,[34] and also the difference in the strength of the electric fields when DC versus AC voltage is applied to the conductive layer of touchscreen. Finally, we show that removing the electrode polarization impedance from the remaining impedance returns the "true" impedance of the air gap and enables us to infer the average thickness of the air gap and the magnitude of electrostatic forces.

Given that direct measurement of the remaining impedance is not feasible, we measure the impedances of dielectrics 1 and 2 in isolation and subtract them from the measured total impedance.[37] This experimental approach is general and valid for almost all applications of EA depicted in Figure 1a. We demonstrate the efficacy of the proposed approach in one of those applications: tactile surfaces where haptic feedback is displayed to human finger through a voltage-induced touchscreen[7,34,39–45] (see **Figure 2**a). It is important to mention that the human finger in this application makes the implementation of the proposed approach more challenging since the factors, such as electroosmosis and electrodermal activity of the skin, can directly affect the impedance measurements. More information on these two phenomena is available in Section SI. 1 (Supporting Information).

2. Results and Discussion

2.1. Physics of Electroadhesion

As shown in Figure 2b, the electric charges and ions in the touchscreen and the finger are distributed randomly when there is no voltage applied to the conductive layer of the touchscreen.

© 2024 The Authors. Advanced Intelligent Systems published by Wiley-VCH GmbH

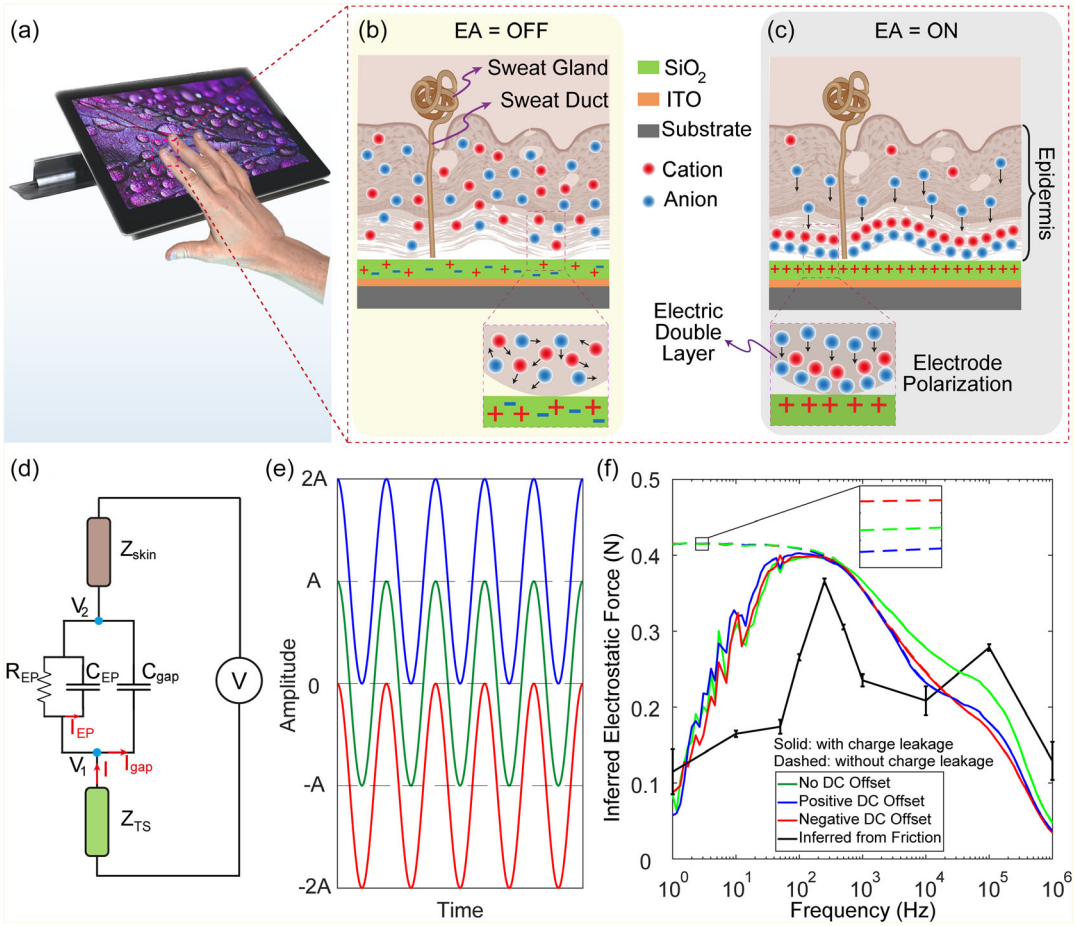


Figure 2. a) A human finger in contact with a touchscreen and b) an enlarged schematic cross-section of the skin–touchscreen interface when EA is OFF. The outermost layer of skin (stratum corneum), which acts as an electrical insulator for the finger, is in contact with the insulator layer of the touchscreen (SiO_2: silicon dioxide) resting on top of a conductor layer (ITO: indium tin oxide). The electrical charges and ions are distributed randomly in both dielectric layers. c) An enlarged schematic cross section of the skin–touchscreen interface when voltage is applied to the conductive layer to generate electrostatic forces between the finger and the touchscreen. The magnitude of these forces is influenced by the electrical impedances of the air gap and the electrode polarization. The electrode polarization occurs due to the EDL at low frequencies. d) Schematic representation of the circuit model proposed for the finger in contact with a touchscreen under EA. e) The three stimuli (the input voltage signal applied to the ITO layer of the touchscreen) used in our study; green, blue, and red colors represent the sinusoidal voltage signals with no, positive, and negative DC offsets, respectively. f) Electrostatic forces inferred from the friction (black-colored curve) and electrical impedance (green, blue, and red-colored solid curves) measurements.

However, when voltage is applied, an electrostatic attraction force builds up between the human finger and the touchscreen due to the parallel plate capacitor principle (see Figure 2c). This principle requires two oppositely charged conductive surfaces, separated by dielectric (insulating) materials. The stratum corneum (SC), which serves as the finger's insulator layer, is primarily made up of dead cells. This layer, similar to all other dielectric materials, can partially prevent the passage of electrical charges. The soft tissue under SC is conductive, and this is why a capacitive touchscreen can detect a finger position in the first place when they are in contact. Similarly, the tactile display (i.e., surface capacitive touchscreen) comprises a thin insulator layer (SiO_2) on top of a conductive layer of indium tin oxide (ITO).

In a recent study, the electrical impedances of human skin and touchscreen were measured separately and subtracted from the total sliding impedance.[37] Hence, the remaining impedance was treated as the air gap impedance, considered in series with the skin and touchscreen impedances. However, we demonstrate in this study that the remaining term represents the impedance of not just the gap between the finger and the touchscreen but also the electrode polarization.[46] Figure 2d shows our proposed schematic circuit model taking into account the effect of electrode polarization. The reason behind electrode polarization is the EDL formed at the contact interface of the finger surface.[38] When the human finger contacts the voltage-induced touchscreen, the ions in the finger tissue are pulled toward the touchscreen's surface and form the first layer on the inner finger surface. This layer comprises ions of opposite charge to that of the touchscreen, while the second layer contains loosely anchored ions of the same charge. The free ions in the finger with opposite charges to those of the touchscreen are attracted to the touchscreen, pushing the ones in the first layer out and

© 2024 The Authors. Advanced Intelligent Systems published by Wiley-VCH GmbH

26404567, 2024, 4, Downloaded from https://onlinelibrary.wiley.com/doi/10.1002/aisy.202300618 by Koc University, Wiley Online Library on [05/07/2024]. See the Terms and Conditions (https://onlinelibrary.wiley.com/terms-and-conditions) on Wiley Online Library for rules of use; OA articles are governed by the applicable Creative Commons License

causing leakage of electrons from the finger to the surface of the touchscreen. At low frequencies below approximately 30 Hz, the free ions have sufficient time to push the ones in the first layer out. Hence, more charges leak and consequently the strength of the electric field at the interface is reduced. The EDL also explains that the electrical behavior of the finger-touchscreen interface is more conductive at low frequencies due to the charge leakage, while more capacitive at high frequencies since the charge leakage diminishes. This clarifies why the strength of the electric field is weaker under DC stimulation compared to AC stimulation. In reference to Figure 2d, the capacitances C_{EP} and C_{gap} short out as the frequency of stimulation approaches zero (i.e., DC condition), and all the current is channeled to the resistance R_{EP}, which results in higher charge leakage compared to that of the AC condition.

For the reason explained above, we performed our impedance measurement under AC stimulation using the input signals shown in Figure 2e. Throughout the paper, we report the results of the impedance measurements performed with sinusoidal voltage signals having positive and negative DC offsets using blue and red-colored curves, respectively, and no DC offset using green-colored curves. The electrostatic forces inferred from our impedance measurements follow a trend similar to those inferred from our friction measurements for frequencies ranging from 1 Hz to 1 MHz (see Figure 2f). Both exhibit an inverted parabolic curve with the highest peak around 250 Hz stimulation frequency and another lower amplitude peak at approximately 100 kHz. A similar inverted parabolic behavior was reported in ref. [47] for the mechanical vibrations of sliding human finger under EA, measured by laser Doppler vibrometer for the stimulation frequencies between 10 Hz and 1 kHz.

2.2. Electrical Impedance Measurements

Our impedance measurements are divided into four groups: 1) electrochemical bioimpedance of human skin; 2) electrical impedance of touchscreen; 3) total electrical impedance of sliding finger on touchscreen; and 4) total electrical impedance of stationary finger on touchscreen.

The average magnitude and phase of the impedance, resistance, and capacitance as a function of frequency with their standard error of means are shown in **Figure 3**a for the skin. The measurements performed with the hydrogel (metal) electrodes are presented in the upper row (lower row). The individual trials are also presented for the hydrogel electrode in Figure S3–S5 (Supporting Information) and the metal electrode in Figure S6–S8 (Supporting Information). It is important to emphasize here that the electrical impedance measurements of human skin may show variations from trial to trial within an individual participant and between different participants as reported for finger skin in earlier studies.[48] The impedance magnitude of skin, similar to its resistance, was found to be higher when measured with metal electrodes compared to hydrogel electrodes due to the effect of electrode polarization impedance. Moreover, the electrode polarization impedance caused phase lag in the impedance response. These results align with the earlier measurements of the skin bioimpedance.[46] The capacitance data show that the dispersion in the skin occurs with the metal electrode at approximately one decade of frequency later than that of the hydrogel electrode. Various polarization mechanisms, which are responsible for different types of dispersions, occur in human skin, but it is not easy to observe all of them since a broad range of frequencies needs to be scanned. In biological materials, α, β, and γ dispersions are typically observed, which are caused by ionic processes, charging up of the membrane or orientation of permanent dipoles, and orientational relaxation, respectively.[49] In our measurements, we do not observe α and γ dispersions since they occur at very low and high frequencies, respectively. We observed β dispersion around 1 kHz for the measurements performed with the hydrogel electrode and around 10 kHz for the measurements performed with the metal electrode. More information on polarization and dispersion is provided in Section SI. 2 (Supporting Information).

Relatively large variations were observed in the impedance magnitude of skin at low frequencies, which is attributed to the influence of electrodermal activity. In fact, measurements of skin bioimpedance at low frequencies are easily influenced by even small movements of the skin, environmental factors, and emotional arousal.[50] Some effect of electro-osmosis (see Section SI. 1, Supporting Information) was also observed in our measurements. The voltage signal with negative DC offset (red-colored curve) resulted in an impedance slightly lower than that of the positive DC offset (blue-colored curve) due to the increase in skin conductance caused by electro-osmosis.[46,51] While both electrodermal activity and electro-osmosis occur at low frequencies, the dominance of electrodermal activity makes the electro-osmosis phenomenon less evident in our results.

The results of the impedance measurements performed on the touchscreen at five different locations on its surface are shown in Figure S10–S14 (Supporting Information) and the average of all measurements, along with their standard error of means, are presented as a function of frequency in Figure 3b. The results suggest that the impedance of the touchscreen does not change significantly with the polarity of the applied voltage signal. Similar to the skin bioimpedance measurements, a dispersion was observed at approximately 10 kHz, which could be related to the electrical properties of the insulating layer of the touchscreen (i.e., SiO_2).

Figure 3c shows the average and standard error of means of the measured total electrical impedance as a function of frequency when the finger was sliding (upper row) and stationary (lower row) on the touchscreen. The results of the individual trials are also reported in Figure S16–S18 and S20–S22 (Supporting Information) for sliding and stationary conditions, respectively. The magnitude of the total impedance measured under the sliding condition is approximately an order of magnitude higher than that of the stationary condition, as observed in ref. [37,52] In the stationary condition, sweat accumulates in the air gap between the finger and the touchscreen and shorts out the air gap impedance due to its high conductivity.[37] However, the finger leaves sweat behind on the touchscreen's surface as it slides, resulting in a higher impedance with respect to the stationary condition. In addition, we also argue that the sweat ducts, together with the skin tissue, contribute to the conduction of current and when the sweat pores of the skin make contact with the surface of touchscreen, sweat acts as a lubricant to increase the conduction through the sweat ducts in the stationary

© 2024 The Authors. Advanced Intelligent Systems published by Wiley-VCH GmbH

26404567, 2024, 4, Downloaded from https://onlinelibrary.wiley.com/doi/10.1002/aisy.202300618 by Koc University, Wiley Online Library on [05/07/2024]. See the Terms and Conditions (https://onlinelibrary.wiley.com/terms-and-conditions) on Wiley Online Library for rules of use; OA articles are governed by the applicable Creative Commons License

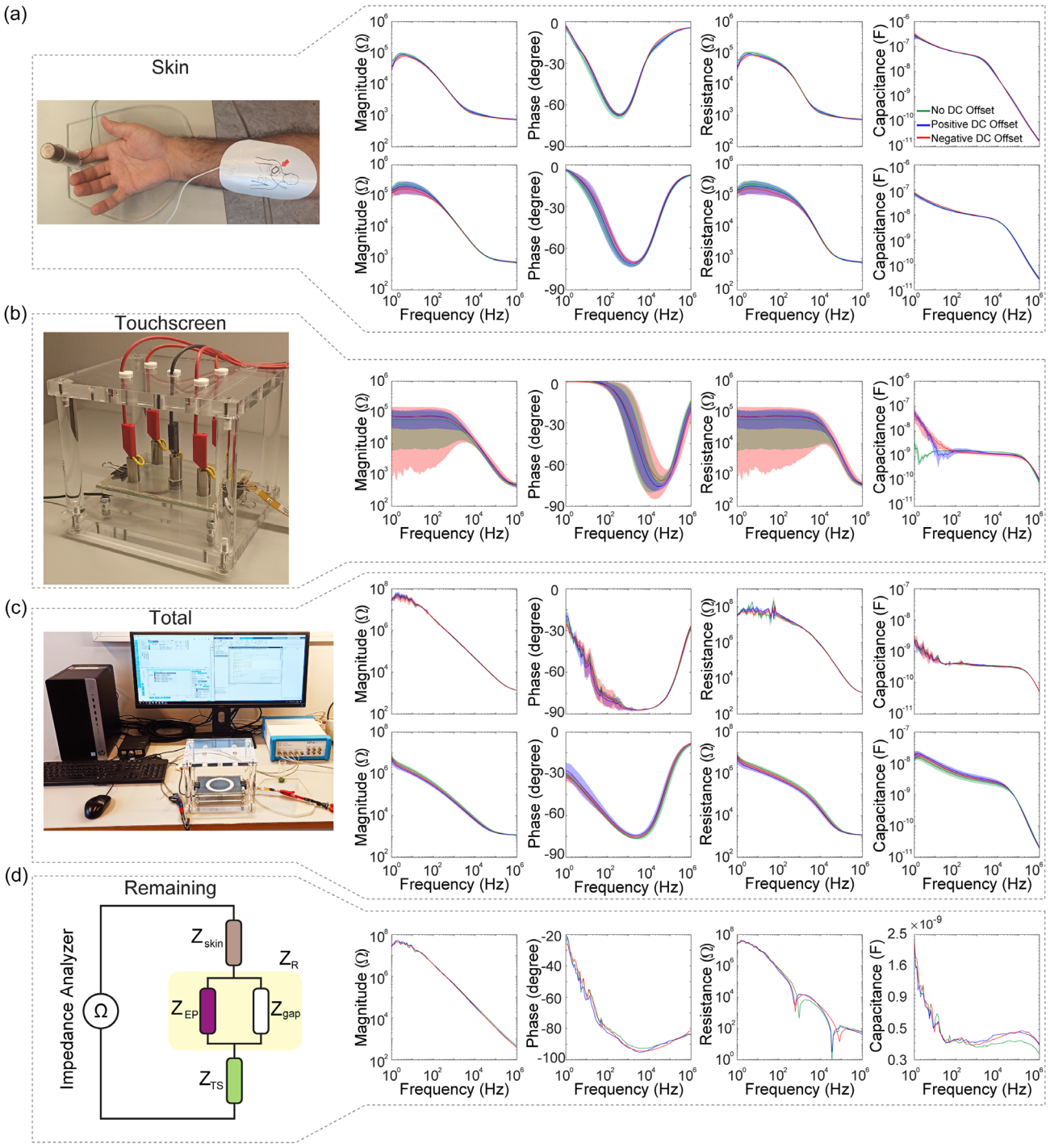


Figure 3. Electrical impedance measurements: The solid curves in the plots represent the mean values of impedance magnitude, phase, resistance, and capacitance as a function of frequency. The shaded regions around the solid curves represent the standard error of means. a) The setup and the measurements for the electrochemical bioimpedance of the skin: the upper (lower) row is for hydrogel (metal) electrode. b) The setup and the measurements for the electrical impedance of the touchscreen in isolation. c) The setup and the measurements for the electrical impedance of finger skin in contact with the touchscreen: the upper (lower) row is for the sliding (stationary) finger. d) The schematic circuit model for the finger–touchscreen interactions: the remaining impedance is calculated by subtracting the measured impedances of skin and touchscreen from the total sliding impedance.

condition. Hence, in the stationary condition, not only does the air gap impedance short out, but the conduction of the skin also increases due to the higher conductivity of the sweat ducts than the soft tissue itself. We believe that these two mechanisms cause a reduction in the total impedance under the stationary condition compared to the sliding one, though more evidence is required to

© 2024 The Authors. Advanced Intelligent Systems published by Wiley-VCH GmbH

26404567, 2024, 4, Downloaded from https://onlinelibrary.wiley.com/doi/10.1002/aisy.202300618 by Koc University, Wiley Online Library on [05/07/2024]. See the Terms and Conditions (https://onlinelibrary.wiley.com/terms-and-conditions) on Wiley Online Library for rules of use; OA articles are governed by the applicable Creative Commons License

support or reject them. Finally, the dispersion in the stationary condition occurred approximately one decade of frequency sooner than that of the sliding condition, which suggests that some polarization mechanisms under the stationary condition failed earlier, weakening the capacitive nature of the contact interface.

The results on phase angle also support the argument that the contact interface shows more capacitive behavior under the sliding condition, as its phase angle levels off just shy of 90° (Figure 3c). The phase plot can be divided into three regions with more resistive behavior at low and high frequencies and more capacitive behavior in the middle. The phase angle for the total stationary impedance follows a similar trend to that of the total sliding impedance, with 20° lower in the middle region. The phase angles of the skin and touchscreen are not only lower than that of the total but also their curves are shifted in phase with respect to that of the total. Their capacitive regions are narrower, and the phase angles for the skin and touchscreen reach their maximum values at approximately 250 Hz and 100 kHz, respectively. Hence, they show the most capacitive behavior at those frequencies.

The results for the remaining impedance, which was calculated by subtracting the skin and touchscreen impedances from the total sliding impedance, are presented in Figure 3d. Moreover, the remaining admittance (inverse of impedance) magnitudes are plotted in **Figure 4**a. A one-decade-per-decade

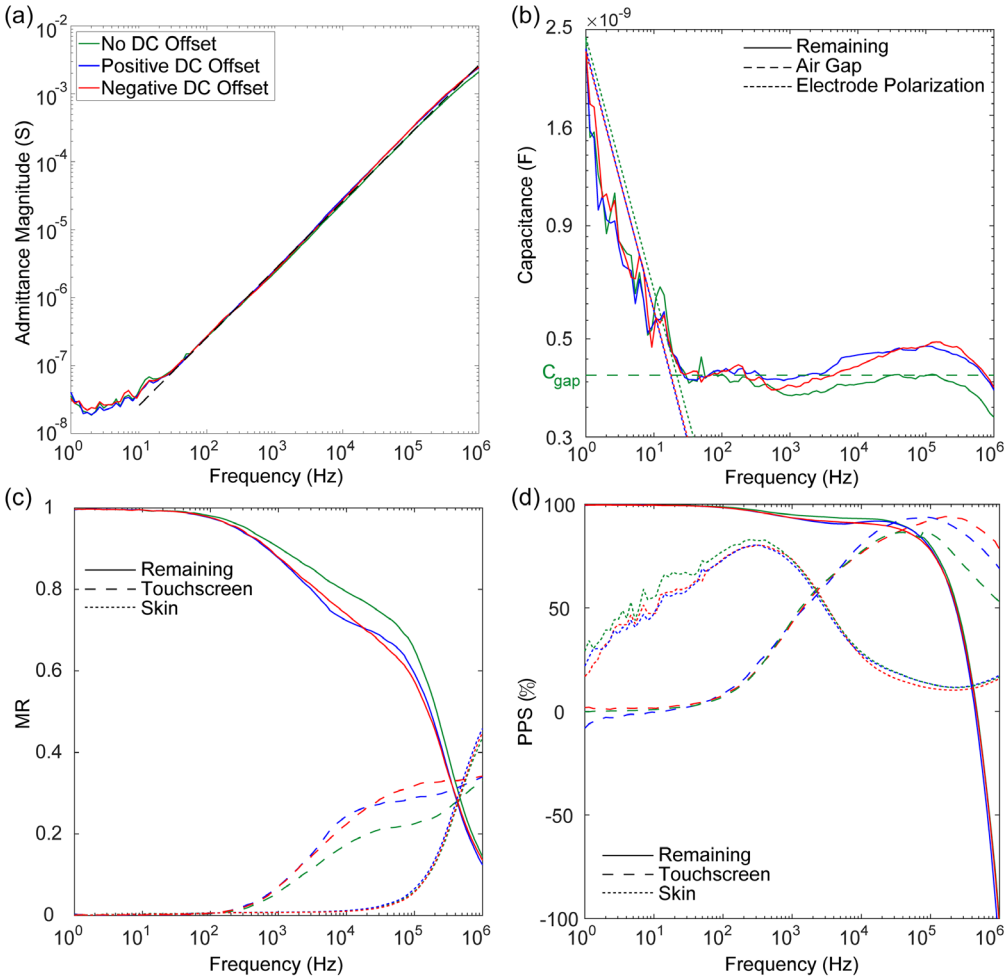


Figure 4. a) The change in remaining admittance as a function of frequency. The dashed line in black color fits the admittance curve well for frequencies higher than approximately 30 Hz, indicating purely capacitive behavior at those frequencies. b) The change in capacitance as a function of frequency. The solid, dashed, and dash-dotted curves in the plot show the capacitances for the remaining term, air gap, and electrode polarization, respectively. The electrode polarization capacitance dominates the remaining capacitance at low frequencies and vanishes afterward. c) MR of each impedance component to the total sliding impedance as a function of frequency. The magnitude of the remaining term dominates the total impedance until approximately 100 kHz, and the touchscreen and skin contribute after 100 Hz and 10 kHz, respectively. The solid, dashed, and dash-dotted curves in the plot show the MR of the remaining term, touchscreen, and skin, respectively. d) Percent phase synchronization (PPS) of each impedance component to that of the total sliding impedance. The phase angle of the remaining impedance is in full synchronization with the total impedance until 100 kHz, and they are asynchronous afterward. The phase angles of skin and touchscreen reach their highest synchronization with the phase angle of the total sliding at approximately 250 Hz and 100 kHz, respectively. The solid, dashed, and dash-dotted curves in the plot show PPS of the remaining term, touchscreen, and skin, respectively.

© 2024 The Authors. Advanced Intelligent Systems published by Wiley-VCH GmbH

26404567, 2024, 4, Downloaded from https://onlinelibrary.wiley.com/doi/10.1002/aisy.202300618 by Koc University, Wiley Online Library on [05/07/2024]. See the Terms and Conditions (https://onlinelibrary.wiley.com/terms-and-conditions) on Wiley Online Library for rules of use; OA articles are governed by the applicable Creative Commons License

26404567, 2024, 4, Downloaded from https://onlinelibrary.wiley.com/doi/10.1002/aisy.202300618 by Koc University, Wiley Online Library on [05/07/2024]. See the Terms and Conditions (https://onlinelibrary.wiley.com/terms-and-conditions) on Wiley Online Library for rules of use; OA articles are governed by the applicable Creative Commons License

line (dotted black) fits the admittance curve well for frequencies larger than 30 Hz. This indicates that the nature of the remaining impedance after this frequency is almost purely capacitive due to the air gap. The phase angle of the remaining impedance also shows that the impedance is more resistive at low frequencies and becomes capacitive at higher frequencies. Hence, the remaining impedance can be modeled by a resistance (R_{EP}) and a capacitance (C_{EP}) in parallel for the electrode polarization and another capacitance parallel to those for the air gap (C_{gap}). We observe that the circuit for the electrode polarization is effective at frequencies lower than 30 Hz while the air gap capacitance dominates the impedance otherwise. In other words, the electrode polarization impedance vanishes after approximately one decade of frequency.[53,54]

2.3. Estimation of Air Gap Thickness

In order to estimate the air gap capacitance from the experimental data, we refer to the remaining admittance (Figure 4a), which is composed of remaining conductance and susceptance. Above 30 Hz, the conductance term almost vanishes, and we can write the remaining admittance as $|Y_R| = B_R/\sin\Phi_R$, where B_R and Φ_R represent the remaining susceptance and phase angle, respectively. At high frequencies, the phase angle is roughly 90°, and hence the remaining admittance equals the remaining susceptance $|Y_R| = B_R = \omega C_R$, where ω and C_R are the frequency of stimulation and the remaining capacitance, respectively. Hence, at frequencies higher than 30 Hz, the remaining capacitance is solely equal to the air gap capacitance, and its value can be calculated by $C_R = C_{gap} = |Y_R|/\omega$. A constant value of $C_{gap} = 413$ pF was obtained using this equation and the experimental data of remaining admittance. The capacitance values of the air gap and the electrode polarization are plotted as a function frequency in Figure 4b. In this figure, the estimated air gap capacitance (413 pF) is represented by a horizontal dashed line in green color.

On the other hand, the capacitance of the air gap is equal to $C_{gap} = \varepsilon_0\varepsilon_{gap}A_{app}/u$, where ε_{gap} is the permittivity of the air (approximately 1.00059) and $A_{app} = 130\,\text{mm}^2$ is the apparent contact area of the participant's index finger, measured by a camera and using image processing methods (see Figure S23, Supporting Information). Substituting these values into the above equation returns the average thickness of the air gap as $u = 2.78$ μm. The lower and upper bounds for the air gap thickness were calculated as 2.57 and 3.28 μm by considering the lowest and highest impedances measured for skin, touchscreen, and the total during sliding. It is worth mentioning here that the thickness of air gap varies from close to zero at the edges of real contact to several micrometers at the places where the separation is largest and the error of assuming a constant (average) separation can be large.

2.4. Inferring Electrostatic Forces from Electrical Impedance Measurements

The earlier approaches in the literature for estimating the electrostatic forces[40,55–57] utilized circuit models without paying attention to the leakage of charges from the finger to the surface of the touchscreen. In our recent study,[34] we inferred the electrostatic forces between a human finger and a voltage-induced touchscreen using an electro-mechanical model that relies on fundamental laws of electric fields. We claimed that considering simple electrical elements such as resistors and capacitors is inadequate to model the true experimentally observed behavior of electrostatic forces changing as a function of frequency. This claim is justified by our current experimental results, where both skin and touchscreen impedances (see Figure 3a,b) exhibit the behavior of a resistor in parallel with a constant phase element (CPE) as suggested earlier.[58] In particular, the phase angle measurements for the skin and the touchscreen in our study cannot be interpreted by a simple circuit model of resistance in parallel with capacitance. Hence, we directly utilized the experimental data of impedance measurements for the skin and touchscreen rather than constructing individual circuit models for them. On the other hand, the behavior of the remaining impedance (see Figure 3d) is relatively easy to interpret, and hence we modeled its behavior using an electrical circuit.

We use Equation (1) to calculate the electrostatic forces as a function of frequency. Since the average air gap was already estimated from the experimental data by the method discussed in Section 2.3, the only unknown in Equation (1) is the voltage across the air gap, which was estimated using the circuit model given in Figure 2d. If an AC voltage (V) with an amplitude V_0 is applied to the conductive layer of the touchscreen, then the total current passing through the system is $I = V/Z_{Total}$ A potential drop occurs across the insulator layers of the touchscreen and skin. Hence, the voltages at nodes 1 and 2 in Figure 2d become $V_1 = V - Z_{TS}I$ and $V_2 = Z_{skin}I$, respectively. Then, the voltage across the remaining impedance, ΔV, is the difference between V_1 and V_2 ($\Delta V = V_1 - V_2$). Since the current passing through R_{EP} equals the difference between the total current (I) and the capacitive currents for the air gap (I_{gap}) and the electrode polarization (I_{EP}), then one can write the potential difference across the air gap as

$$\Delta V_{gap} = \Delta V - R_{EP}\left[I - \left(I_{gap} + I_{EP}\right)\right] \tag{2}$$

Substituting Equation (2) into Maxwell's stress tensor (Equation (1)) gives the electrostatic forces, which are plotted in Figure 2f as a function of frequency for $V_0 = 75$ Volts. The magnitude of electrostatic forces increases with the stimulation frequency reaching a peak value at 250 Hz and decreases afterward. A smaller peak also occurs at 100 kHz. The dashed curves in the figure represent the case in which the electrode polarization was not considered in the model (i.e., the charge leakage from the finger to the surface of the touchscreen was not taken into account). Under this circumstance, the magnitude of electrostatic forces is high and constant until 250 Hz and then drops. This supports our earlier findings,[34] suggesting that charge leakage is the dominant factor in reducing the magnitude of electrostatic forces at low frequencies.

In order to further investigate the frequency-dependent behavior of electrostatic forces, we analyze the relative contribution of each impedance (skin, touchscreen, and remaining) to the total sliding impedance. First, the ratio of magnitudes of each impedance to the total sliding impedance was calculated by[37]

© 2024 The Authors. Advanced Intelligent Systems published by Wiley-VCH GmbH

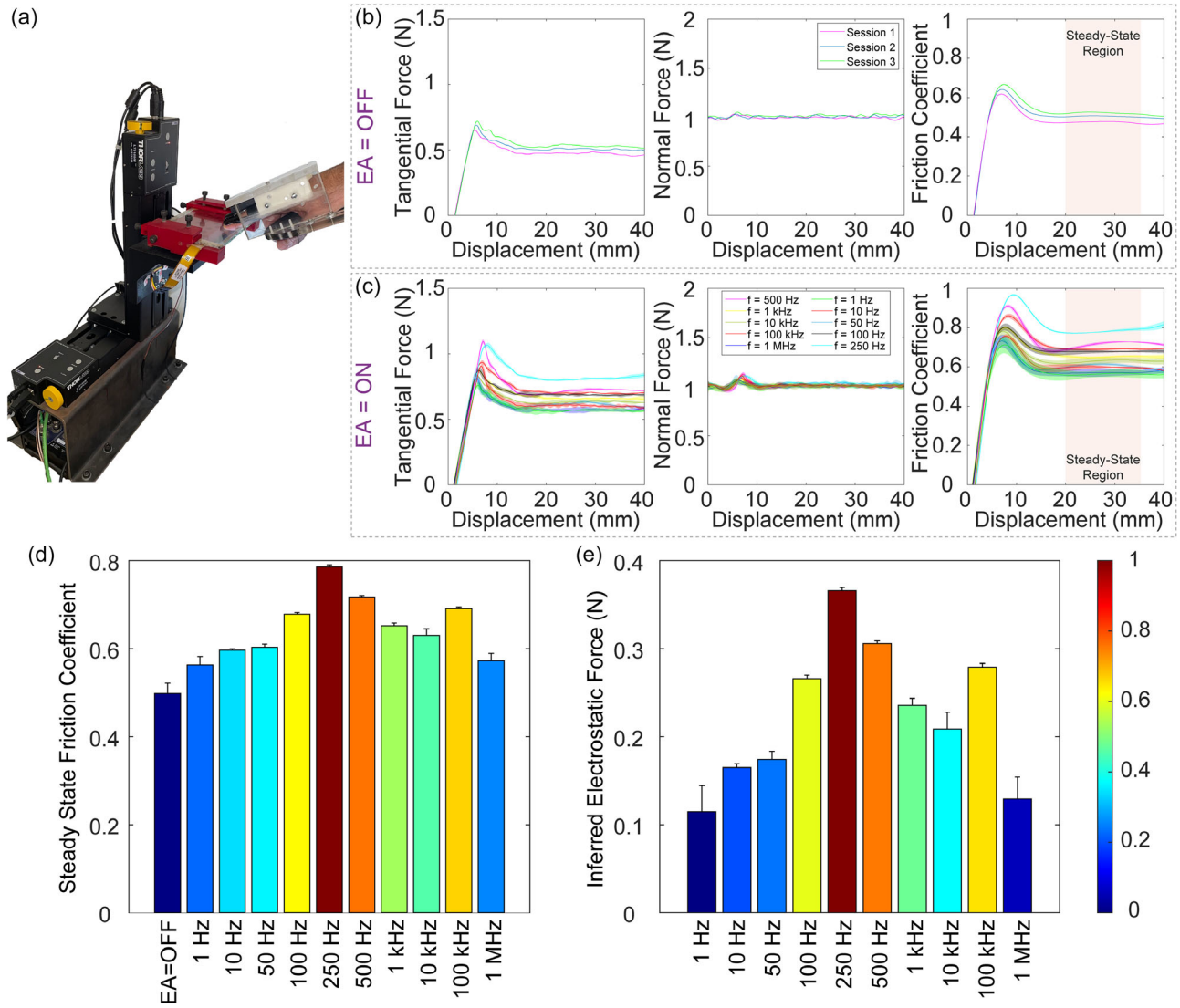


Figure 5. a) The setup for measuring frictional forces between the participant's index finger and the touchscreen. The participant's finger was stationary, and the touchscreen was translated beneath the finger with a constant velocity. The normal and tangential forces acting on the finger were measured using a force sensor placed under the touchscreen. The normal forces were maintained at 1 N using a PID controller. b) The mean values of tangential and normal forces acting on the participant's index finger and the CoF as a function of displacement when EA was turned off (EA = OFF). c) The mean values of tangential and normal forces acting on the participant's index finger and the CoF as a function of displacement when EA was turned on (EA = ON). Sinusoidal voltage signals at ten different frequencies with an amplitude of 75 Volts were applied to the conductive layer of the touchscreen to generate electrostatic forces between the finger and the touchscreen. d) The mean values of steady-state CoF when EA = OFF and for the ten stimulation frequencies when EA = ON. e) The mean values of electrostatic forces as a function of stimulation frequency when EA = ON.

$$\mathrm{MR}_i = \frac{Z_i}{Z_{\mathrm{Total(Sliding)}}} \tag{3}$$

$$\mathrm{PPS}_i = \left[1 - \frac{|\Phi_i - \Phi_{\mathrm{Total(Sliding)}}|}{|\Phi_{\mathrm{Total(Sliding)}}|}\right] \times 100 \tag{4}$$

where, i indicates each component (skin, touchscreen, remaining). The results (Figure 4c) show that the remaining impedance contributes the most to the total impedance until 100 kHz. The touchscreen and skin start to contribute to the total impedance after 100 Hz and 10 kHz, respectively. Second, we analyze how well the phase of each impedance (skin, touchscreen, remaining) was synchronized with that of the total sliding impedance using the following metric

where PPS_i represents the percent phase synchronization (PPS) of the impedance component i with the phase of the total sliding impedance. As shown in Figure 4d, the phase of the remaining impedance is highly synchronized with that of the total sliding impedance until 100 kHz, where a sharp asynchronization starts afterward. The phases of the skin and touchscreen are most synchronized with the phase of the total at approximately 250 Hz and 100 kHz, respectively. Based on the MR and PPS plots

© 2024 The Authors. Advanced Intelligent Systems published by Wiley-VCH GmbH

26404567, 2024, 4, Downloaded from https://onlinelibrary.wiley.com/doi/10.1002/aisy.202300618 by Koc University, Wiley Online Library on [05/07/2024]. See the Terms and Conditions (https://onlinelibrary.wiley.com/terms-and-conditions) on Wiley Online Library for rules of use; OA articles are governed by the applicable Creative Commons License

and our earlier findings, we claim that the air gap impedance dominates the total sliding impedance for a broad range of stimulation frequencies (from approximately 30 Hz to 100 kHz). Moreover, the two peak amplitudes observed at 250 Hz and 100 kHz in our estimation of electrostatic forces based on friction measurements (see Figure 2f) match with the peaks observed in the PPS curves for the skin and touchscreen impedances (see Figure 4d), respectively. We argue that the synchronization of the skin phase at 250 Hz and the touchscreen phase at 100 kHz with the phase of the total impedance amplifies the strength of the electric field at those frequencies, resulting in high amplitudes in electrostatic forces.

2.5. Inferring Electrostatic Forces from Friction Measurements

The electrostatic forces inferred from the impedance measurements were compared with the ones inferred from friction measurements performed by the set-up shown in **Figure 5**a. The average tangential and normal forces and the friction coefficients (CoF) are presented in Figure 5b,c as a function of relative displacement between finger and the touchscreen for EA = OFF and EA = ON conditions, respectively. Note that the results of individual trials for tangential and normal forces and CoF are reported in Figure S24 and S25 (Supporting Information), respectively. The steady-state values of CoF are shown in Figure 5d, and the electrostatic forces inferred from friction measurements are presented in Figure 5e. The electrostatic forces inferred from friction and electrical impedance measurements are in good agreement, as shown in Figure 2f. They both exhibit an inverted parabolic behavior where the electrostatic forces increase until approximately 250 Hz and drop afterward, with another peak at approximately 100 kHz.

3. Conclusion

Due to its unique features, EA technology has already been utilized in many applications in different domains so far. However, our understanding of the physics behind it is still highly limited. Although controlling the magnitude of attractive electrostatic force that holds two surfaces together is critical in many applications of EA, the effects of the input voltage signal (amplitude and frequency), and several other internal (e.g., electrical and mechanical properties of the contacting surfaces) and external (e.g., humidity and temperature) factors on this force are not fully known yet. Furthermore, since the contacting surfaces have finite roughness, there is an air gap between them which varies from a few nanometers to a few micrometers across the contact area and makes it difficult to measure the electrostatic forces directly. In this article, we proposed an alternative approach based on the measurement of electrical impedances to experimentally infer the air gap thickness first and then the magnitude of electrostatic forces. We measured the electrical impedances of the contacting surfaces and subtracted them from the total impedance to obtain the remaining impedance. Then, we extracted the air gap impedance from the remaining impedance by removing the undesired effects of electrode polarization impedance. We showed that the electrode polarization impedance is effective at low frequencies, and it is not possible to estimate the electrostatic forces correctly without filtering out its effect from the remaining impedance. Although we demonstrated the application of our proposed approach in contact interactions of the human finger with a tactile surface, we should emphasize that electrode polarization is not exclusive to the electrical measurements performed on biological structures only, such as human skin in our application. It can also occur in all other EA applications involving two contacting surfaces with different electrical properties.

In terms of our application, our electrical impedance measurements revealed new information about the physics of finger interactions with a tactile surface under EA, which has not been published before. In our earlier modeling studies,[34,42] we claimed that the charge leakage from the finger to the surface of the touchscreen is the main cause of the reduction in electrostatic forces for frequencies below 30 Hz. Our current study provides an experimental evidence for this claim. As shown in Figure 2f, the electrostatic forces inferred by the impedance measurements are low (high) when the charge leakage is taken (not) into account. We argue that an EDL builds up at the contact interface of the finger surface (Figure 2c) and causes the electrons to leak to the surface of the touchscreen. Furthermore, our analysis based on magnitude ratio (MR) and phase synchronization (PPS) shows that finger skin (touchscreen) contributes most to the total impedance at 250 Hz (10 kHz) frequencies (Figure 4c,d). Surprisingly, the electrostatic forces inferred from the friction measurements also attain peak values at those frequencies (see the black-colored solid lines in Figure 2f). This suggests that not only the electrical properties of the finger skin but also those of the insulator layer of the touchscreen play a role in the magnitude of electrostatic forces. Although the earlier modeling studies[7,34,42,55–57] took into account the frequency-dependent permittivity and resistivity of SC, constant values were considered for the insulator layer of touchscreen (SiO_2). However, our impedance measurements performed on the touchscreen showed otherwise (see Figure 3b). Finally, the circuit model based on the experimental impedance measurements (Figure 2d) explains the difference between the DC and AC stimulation conditions. It shows that the interface becomes purely resistive and cannot successfully store electrical energy as the frequency approaches zero (DC), resulting in a weak electrical field and electrostatic forces.

4. Experimental Section

Participants: One healthy right-handed participant (30 years old) was selected to take part in this study. A consent form was read and signed by the participant before the experiment, which was approved by the Ethical Committee for Human Participants of Koc University. The study conformed to the principles of the Declaration of Helsinki, and the experiment was performed following relevant guidelines and regulations.

Since emotions can alter the psychological sweating mechanism, the participant was asked to inform the experimenter regarding his emotional feelings and any pains or aches in his body before starting the experiments. Stress, anxiety, discomfort, excitement, and sleeplessness could be the factors affecting any electrical measurements involving the human skin. Before each experimental trial, the participant washed his hands with soap, rinsed with water, and dried them with a clean towel. He also waited in the experimentation room for 5 min without touching anything before each trial. This protocol was strictly followed for all trials to ensure that the

© 2024 The Authors. Advanced Intelligent Systems published by Wiley-VCH GmbH

26404567, 2024, 4, Downloaded from https://onlinelibrary.wiley.com/doi/10.1002/aisy.202300618 by Koc University, Wiley Online Library on [05/07/2024]. See the Terms and Conditions (https://onlinelibrary.wiley.com/terms-and-conditions) on Wiley Online Library for rules of use; OA articles are governed by the applicable Creative Commons License

26404567, 2024, 4, Downloaded from https://onlinelibrary.wiley.com/doi/10.1002/aisy.202300618 by Koc University, Wiley Online Library on [05/07/2024]. See the Terms and Conditions (https://onlinelibrary.wiley.com/terms-and-conditions) on Wiley Online Library for rules of use; OA articles are governed by the applicable Creative Commons License

sebum or sweat from the finger's surface was removed and the skin had enough time to reach its normal hydration level.

Apparatus for Measuring Electrical Impedance: In all electrical impedance measurements performed by an impedance analyzer (MFIA 5 MHz, Zurich Instruments Inc.), the four-electrode method was chosen. Since electrical impedance measurements are prone to noise, the impedance analyzer was calibrated before each measurement session: 1) The electrochemical bioimpedance of the skin was measured using two types of electrodes: hydrogel and metal electrodes. The measurements were performed in three separate sessions on three different days, and the data were collected in ten consecutive trials (10 trials/session $\times$ 3 sessions). Figure S2 (Supporting Information) presents the experimental apparatus for the bioimpedance measurements. A small hydrogel electrode (1050NPSM Neonatal Pre Wired Small Cloth ECG Electrodes, Cardinal Health Inc.) was attached to the participant's right-hand index finger. A larger electrode (HeartStart FR2 Defibrillation Electrode Pads, Philips Medical Systems Inc.) was attached to the ventral forearm of the same hand. This electrode has a contact area approximately ten times larger than the small electrode to minimize its contribution to bioimpedance measurements. During the measurements, the applied current always entered the skin through one electrode and exited it from the other depending on the polarity of the signal. We replaced the hydrogel electrode with a metal one and repeated the impedance measurements. The hydrogel electrode has a solid gel layer that reduces the electrode polarization effects. A weight of 100 g, equivalent to a normal force of 1 N, was placed on top of the small electrode at the fingertip and kept vertically aligned using a custom-made circular tube; 2) The electrical impedance of the touchscreen was measured using a set of five custom-made metal electrodes (see Figure S9a, Supporting Information). The electrodes were attached to the touchscreen's surface at five different locations using a very thin layer of silver grease (8463A, MG Chemicals). The data were collected in ten consecutive trials from each location (10 trials/location $\times$ 5 locations). The electrode locations were selected to cover the whole surface of the touchscreen. In a pilot study, we observed that the impedance measurements were sensitive to the thickness of the silver grease between the electrodes and the touchscreen. Efforts were made to perform the measurements with the thinnest possible layer of silver grease, but this approach resulted in relatively large variations in the impedance measurements. A support structure was also manufactured to keep the connection cables stable and minimize the electrical noise (see Figure S9b, Supporting Information); 3) The total electrical impedance of the finger was measured while the participant's finger was sliding on the surface of the touchscreen (i.e., sliding condition). The measurements were performed in three separate sessions on three different days, and the data were collected in ten consecutive trials (10 trials/session $\times$ 3 sessions). A user interface was developed in MATLAB (The MathWorks Inc.) to provide visual feedback to the participant while his finger made circular movements on the surface of the touchscreen. As shown in Figure S15 (Supporting Information), the black-colored cursor displayed on the computer monitor circled on the dashed-green trajectory ($r = 4$ cm) with a constant velocity of 40 mm s^{-1}. The participant was asked to follow the cursor's motion by moving his finger on the touchscreen at the desired speed. A circular trajectory of the same size as the dashed-green trajectory was printed on paper and placed beneath the touchscreen to help the subject follow it more easily. The blue bar on the computer monitor displayed the magnitude of normal force applied by the participant's finger to the touchscreen in real time. Two horizontal green-dashed lines at 0.8 and 1.2 N showed the lower and higher limits of the normal force to assist the participant control his normal force close to 1 N. The normal force was measured using a force transducer (Nano17-SI-12-0.12, ATI Inc.) placed beneath the touchscreen and acquired by a data acquisition card (PCIe-6034E, National Instruments Inc.) at 100 Hz. The participant was trained before the experiment to get familiar with the procedure. He could maintain the normal force close to the desired value while moving his finger on the circle (1 ± 0.15 N); and 4) We measured the total electrical impedance of the finger while it is stationary on the touchscreen (see Figure S19, Supporting Information). The measurements were performed in three separate sessions on three different days, and the data were collected in ten consecutive trials (10 trials/session $\times$ 3 sessions). The data were collected from five different sites on the touchscreen, and the participant was instructed to change the location of his finger after every two trials. The participant was asked to keep his finger stable during the measurements while trying to maintain the normal force close to the desired value.

Calculation of the Remaining Impedance: Since electrical impedances of skin, touchscreen, and the remaining are assumed to be in series based on the model shown in Figure 3d, the skin (Z_{skin}) and touchscreen (Z_{TS}) impedances were subtracted from the total sliding impedance ($Z_{Total(Sliding)}$) to obtain the remaining impedance using the following equation

$$Z_R = Z_{Total(Sliding)} - Z_{skin} - Z_{TS} \tag{5}$$

It is essential to insert real and imaginary parts of the measured impedances into this equation. Otherwise, it is not possible to calculate the phase angle of the remaining impedance or its resistance/capacitance.

Apparatus for Measuring Frictional Forces: The present study employs the experimental setup (see Figure S23a, Supporting Information) developed in ref. [34,59] for friction measurements. It consists of a capacitive touchscreen (SCT3250, 3M Inc.) and a force transducer (Mini40-SI-80-4, ATI Inc.) placed beneath it to measure normal and tangential forces acting on the finger. The setup also includes two linear translational stages (LTS150, Thorlabs Inc.) to move the touchscreen with respect to the finger in normal and tangential directions and a waveform generator (33220A, Agilent Inc.) connected to a piezo driver/amplifier (PZD700A M/S, Trek Inc.) to apply a voltage signal to the touchscreen. A DAQ card (PCIe-6034E, National Instruments Inc.) was utilized to acquire the normal and tangential forces acting on the finger at 2.5 kHz. We measured the CoF between the finger and touchscreen for sinusoidal input voltage signals having an amplitude of 75 volts and at different stimulation frequencies varying from 1 Hz to 1 MHz (1 Hz, 10 Hz, 50 Hz, 100 Hz, 250 Hz, 500 Hz, 1 kHz, 10 kHz, 100 kHz, and 1 MHz). We also measured the CoF for the case where there was no EA. The experiments were performed in three sessions on three separate days. Each stimulation condition was repeated three times in each session. Hence, a total of ninty trials were performed for EA = ON (3 sessions $\times$ 10 frequencies $\times$ 3 repetitions/frequency) and nine trials for EA = OFF (3 sessions $\times$ 3 repetitions). During the experiments, the normal force acting on the finger was kept constant at 1 N using a PID controller and the vertical stage. Then, the horizontal stage was commanded to move 40 mm under the finger in the tangential direction. Its velocity profile is presented in Figure S23b (Supporting Information). The first and last 5 mm displacements reflected the acceleration and deceleration phases of the movement. The CoF was calculated by dividing the recorded tangential forces by normal forces. The steady-state region for CoF was taken as the displacement interval from 20 to 35 mm. Using the average values of CoF in that interval, the electrostatic forces were calculated by[60]

$$F_e = \left(1 - \frac{\mu^{OFF}}{\mu^{ON}}\right) F_n \tag{6}$$

where μ is the steady-state CoF and F_n is the normal force acting on the participant's finger.

Supporting Information

Supporting Information is available from the Wiley Online Library or from the author.

Acknowledgements

E.A. and C.B. acknowledge the financial support provided by the Scientific and Technological Research Council of Turkey (TUBITAK) under contract numbers 117E954 and 123E138. E.A. acknowledges the academic visit to

© 2024 The Authors. Advanced Intelligent Systems published by Wiley-VCH GmbH

University of Oslo, which was supported by O.G.M., Erasmus student exchange program, and Koc University. E.A. is also grateful to Seyed Morteza Hoseyni for the discussions related to the mechanical vibrations.

Conflict of Interest

The authors declare no conflict of interest.

Data Availability Statement

The data that support the findings of this study are available from the corresponding author upon reasonable request.

Keywords

interfacial air gap, bioimpedance, electrical impedance, electroadhesion, polarization, robotics, tactile displays

Received: October 3, 2023
Revised: November 30, 2023
Published online: February 16, 2024

[1] J. Shintake, V. Cacucciolo, D. Floreano, H. Shea, *Adv. Mater.* **2018**, *30*, 1707035.
[2] D. J. Levine, K. T. Turner, J. H. Pikul, *Adv. Mater.* **2021**, *33*, 2007952.
[3] P. Rajagopalan, M. Muthu, Y. Liu, J. Luo, X. Wang, C. Wan, *Adv. Intell. Syst.* **2022**, *4*, 2200064.
[4] A. Johnsen, K. Rahbek, *J. Inst. Electr. Eng.* **1923**, *61*, 713.
[5] E. Mallinckrodt, A. Hughes, W. Sleator Jr, *Science* **1953**, *118*, 277.
[6] J. Shintake, S. Rosset, B. Schubert, D. Floreano, H. Shea, *Adv. Mater.* **2016**, *28*, 231.
[7] M. Ayyildiz, M. Scaraggi, O. Sirin, C. Basdogan, B. N. Persson, *Proc. Natl. Acad. Sci.* **2018**, *115*, 12668.
[8] H. J. Kim, L. Paquin, C. W. Barney, S. So, B. Chen, Z. Suo, A. J. Crosby, R. C. Hayward, *Adv. Mater.* **2020**, *32*, 2000600.
[9] C. Basdogan, F. Giraud, V. Levesque, S. Choi, *IEEE Trans. Haptic* **2020**, *13*, 450.
[10] T.-H. Yang, J. R. Kim, H. Jin, H. Gil, J.-H. Koo, H. J. Kim, *Adv. Funct. Mater.* **2021**, *31*, 2008831.
[11] Y. Liu, P. Wang, X. Su, L. Xu, Z. Tian, H. Wang, G. Ji, J. Huang, *Adv. Mater.* **2022**, *34*, 2108820.
[12] J. Wang, A. Chortos, *Adv. Intell. Syst.* **2022**, *4*, 2100165.
[13] Z. Liu, F. Yan, *Adv. Sci.* **2022**, *9*, 2200264.
[14] G. Monkman, *Ind. Rob.* **2003**, *30*, 326.
[15] G. Beasley, W. Hankins, in *Weightlessness and Artificial Gravity Meeting*, American Institution of Aeronautics and Astronautics, Williamsburg, VA **1971**, p. 853.
[16] T. Bryan, T. Macleod, L. Gagliano, S. Williams, B. McCoy, in *Advanced Maui Optical and Space Surveillance Technologies Conf., M15-4855*, SAO/NASA Astrophysics Data System, Maui, HI **2015**, pp. 1–8.
[17] B. C. Leung, N. R. Goeser, L. A. Miller, S. Gonzalez, in *IEEE Aerospace Conf.*, IEEE, Piscataway, NJ **2015**, pp. 1–8.
[18] G. A. Wardly, *Rev. Sci. Instrum.* **1973**, *44*, 1506.
[19] K. Yatsuzuka, J.-I. Toukairin, K. Asano, S. Aonuma, in *Conf. Record of the 2001 IEEE Industry Applications Conf. 36th IAS Annual Meeting (Cat. No. 01CH37248)*, Vol. *1*, IEEE, Piscataway, NJ **2001**, pp. 399–403.
[20] K. Asano, F. Hatakeyama, K. Yatsuzuka, *IEEE Trans. Ind. Appl.* **2002**, *38*, 840.
[21] G. J. Monkman, P. M. Taylor, G. Farnworth, *Int. J. Clothing Sci. Technol.* **1989**, *1*, 14.
[22] G. J. Monkman, *Int. J. Rob. Res.* **1995**, *14*, 144.
[23] Z. Zhang, *IEEE/ASME Trans. Mechatron.* **1999**, *4*, 39.
[24] A. Yamamoto, T. Nakashima, T. Higuchi, in *Int. Symp. on Micro-NanoMechatronics and Human Science*, IEEE, Piscataway, NJ **2007**, pp. 389–394.
[25] H. Prahlad, R. Pelrine, S. Stanford, J. Marlow, R. Kornbluh, in *IEEE Int. Conf. on Robotics and Automation*, IEEE, Piscataway, NJ **2008**, pp. 3028–3033.
[26] H. Wang, A. Yamamoto, T. Higuchi, *Int. J. Adv. Rob. Syst.* **2014**, *11*, 191.
[27] Q. Wu, V. Pradeep, X. Liu, In *IEEE Int. Conf. on Soft Robotics (RoboSoft)*, IEEE, Piscataway, NJ **2018**, pp. 315–320.
[28] J. Germann, B. Schubert, D. Floreano, in *2014 IEEE/RSJ Int. Conf. on Intelligent Robots and Systems*, IEEE, Piscataway, NJ **2014**, pp. 3933–3938.
[29] V. Cacucciolo, H. Shea, G. Carbone, *Extreme Mech. Lett.* **2022**, *50*, 101529.
[30] Y. Piskarev, A. Devincenti, V. Ramachandran, P.-E. Bourban, M. D. Dickey, J. Shintake, D. Floreano, *Adv. Intell. Syst.* **2023**, *5*, 2200409.
[31] J. Guo, J. Leng, J. Rossiter, *IEEE Trans. Rob.* **2019**, *36*, 313.
[32] M. A. Graule, P. Chirarattananon, S. B. Fuller, N. T. Jafferis, K. Y. Ma, M. Spenko, R. Kornbluh, R. J. Wood, *Science* **2016**, *352*, 978.
[33] B. N. Persson, *J. Phys.: Condens. Matter* **2021**, *43*, 435001.
[34] E. AliAbbasi, M. A. Sormoli, C. Basdogan, *IEEE Trans. Haptic* **2022**, *15*, 416.
[35] D. K. Cheng, *Field and Wave Electromagnetics*, Pearson Education, Inc., China **1989**.
[36] B. N. Persson, *J. Chem. Phys.* **2001**, *115*, 3840.
[37] C. D. Shultz, M. Peshkin, J. E. Colgate, in *IEEE Haptics Symp. (HAPTICS)*, IEEE, Piscataway, NJ **2018**, pp. 151–157.
[38] W. Kuang, S. Nelson, *Trans. ASAE* **1968**, *14*, 173.
[39] O. Bau, I. Poupyrev, A. Israr, C. Harrison, in *Proc. of the 23rd Annual ACM Symp. on User Interface Software and Technology*, Association for Computing Machinery, New York, NY **2010**, pp. 283–292.
[40] D. J. Meyer, M. A. Peshkin, J. E. Colgate, in *World Haptics Conf. (WHC)*, IEEE, Piscataway, NJ **2013**, pp. 43–48.
[41] Y. Vardar, B. Güçlü, C. Basdogan, *IEEE Trans. Haptic* **2017**, *10*, 488.
[42] O. Sirin, M. Ayyildiz, B. Persson, C. Basdogan, *Soft Matter* **2019**, *15*, 1758.
[43] J. E. Colgate, M. A. Peshkin, US Patent 10,379,655 **2019**.
[44] X. Li, Y. Ma, C. Choi, X. Ma, S. Chatterjee, S. Lan, M. C. Hipwell, *Adv. Mater.* **2021**, *33*, 2008337.
[45] G. Lee, C. Park, D. Park, S. Choi, U. Jeong, *Adv. Opt. Mater.* **2023**, *11*, 2202515.
[46] S. Grimnes, O. G. Martinsen, *Bioimpedance and Bioelectricity Basics*, 3rd ed., Academic Press, London, UK **2015**.
[47] R. F. Friesen, R. L. Klatzky, M. A. Peshkin, J. E. Colgate, *IEEE Trans. Haptic* **2021**, *14*, 897.
[48] X. Zou, C. Chen, T. Liang, J. Xie, E.-N. Gillette-Henao, J. Oh, J. Tumalle, A. D. Mazzeo, *Adv. Electron. Mater.* **2018**, *4*, 1800131.
[49] H. P. Schwan, S. Takashima, *Bull. Inst. Chem. Res., Kyoto Univ.* **1991**, *69*, 459.
[50] W. Boucsein, *Electrodermal Activity*, 2nd ed., Springer Science & Business Media, New York, NY **2012**.
[51] S. Grimnes, *Med. Biol. Eng. Comput.* **1983**, *21*, 739.
[52] Y. Vardar, K. J. Kuchenbecker, *J. R. Soc. Interface* **2021**, *18*, 20200783.
[53] H. Schwan, *Ann. N. Y. Acad. Sci.* **1968**, *148*, 191.
[54] H. Schwan, *Ann. Biomed. Eng.* **1992**, *20*, 269.
[55] E. Vezzoli, M. Amberg, F. Giraud, B. Lemaire-Semail, in *Int. Conf. on Human Haptic Sensing and Touch Enabled Computer Applications*, Springer, Versailles, France **2014**, pp. 369–376.

© 2024 The Authors. Advanced Intelligent Systems published by Wiley-VCH GmbH

26404567, 2024, 4, Downloaded from https://onlinelibrary.wiley.com/doi/10.1002/aisy.202300618 by Koc University, Wiley Online Library on [05/07/2024]. See the Terms and Conditions (https://onlinelibrary.wiley.com/terms-and-conditions) on Wiley Online Library for rules of use; OA articles are governed by the applicable Creative Commons License

[56] Y. Vardar, B. Güçlü, C. Basdogan, in *Int. Conf. on Human Haptic Sensing and Touch Enabled Computer Applications*, Springer, London, UK **2016**, pp. 190–203.
[57] F. Forsbach, M. Heß, *Facta Univ. Ser.: Mech. Eng.* **2021**, *19*, 39.
[58] V. F. Lvovich, *Impedance Spectroscopy: Applications to Electrochemical and Dielectric Phenomena*, John Wiley & Sons, Inc., Hoboken, New Jersey **2012**.
[59] I. Ozdamar, M. R. Alipour, B. P. Delhaye, P. Lefevre, C. Basdogan, *IEEE Trans. Haptic* **2020**, *13*, 137.
[60] C. Basdogan, M. A. Sormoli, O. Sirin, *IEEE Trans. Haptic* **2020**, *13*, 511.
[61] J. Xiao, H. Wang, *Contemporary Issues in Systems Science and Engineering*, John Wiley & Sons, Inc., Hoboken, New Jersey **2015**, pp. 737–766.
[62] K. H. Koh, M. Sreekumar, S. Ponnambalam, *Mechatronics* **2016**, *35*, 122.

© 2024 The Authors. Advanced Intelligent Systems published by Wiley-VCH GmbH

26404567, 2024, 4, Downloaded from https://onlinelibrary.wiley.com/doi/10.1002/aisy.202300618 by Koc University, Wiley Online Library on [05/07/2024]. See the Terms and Conditions (https://onlinelibrary.wiley.com/terms-and-conditions) on Wiley Online Library for rules of use; OA articles are governed by the applicable Creative Commons License